CHINESE OPTICS LETTERS

Vol. 20, No. 6 | June 2022

1.65 μm square-FP coupled cavity semiconductor laser for methane gas detection

Yingrun Fan (樊碘润)[1,2], Jinlong Xiao (肖金龙)[2,3*], Zhengzheng Shen (沈征征)[2,3], Youzeng Hao (郝友增)[2,3], Jiachen Liu (刘家辰)[2,3], Ke Yang (杨 珂)[2,3], Yuede Yang (杨跃德)[2,3], and Yongzhen Huang (黄永箴)[1,2,3]

[1] School of Microelectronics, University of Chinese Academy of Sciences, Beijing 100049, China

[2] State Key Laboratory of Integrated Optoelectronics, Institute of Semiconductors, Chinese Academy of Sciences, Beijing 100083, China

[3] Center of Materials Science and Optoelectronics Engineering, University of Chinese Academy of Sciences, Beijing 100049, China

*Corresponding author: jlxiao@semi.ac.cn

Received January 19, 2022 | Accepted March 25, 2022 | Posted Online April 27, 2022

We report a 1.65 μm square-Fabry–Pérot (FP) coupled cavity semiconductor laser for methane gas detection. The laser output optical power can reach 7.4 mW with the side mode suppression ratio about 40 dB. The wavelength tuning range is 2 nm by adjusting the FP cavity injection current, covering the methane absorption line at 1653.72 nm. The lasing wavelength can also be tuned by adjusting the square microcavity injection current or temperature, respectively. Methane gas detection is successfully demonstrated utilizing this laser.

Keywords: coupled cavity lasers; tunable lasers; tunable diode laser absorption spectroscopy; methane gas detection.
DOI: 10.3788/COL202220.061401

1. Introduction

Tunable diode laser absorption spectroscopy (TDLAS) technology utilizes the narrow linewidth and wavelength tunability of semiconductor lasers to realize gas detection in real time and has the advantages of noncontact, high resolution, high sensitivity, and fast response time[1–9]. In recent years, many tunable semiconductor lasers suitable as the light source for gas detection systems based on TDLAS technology have been reported[10–21]. Yu *et al.* demonstrated widely tunable distributed Bragg reflector (DBR) lasers for multispecies gas sensing. Utilizing these DBR lasers, the water and methane detection experiment has been successfully implemented[11–13]. Wang *et al.* designed and implemented a near-infrared methane detection system based on TDLAS technology using a distributed feedback laser at 1654 nm. The system allows real-time display and has the potential of adjustable wavelength scanning for multi-gas detection[15]. Meng *et al.* reported a micro-ring resonator laser based on whispering-gallery modes (WGMs) with an annular resonator and an output waveguide at 1746.4 nm. It is a promising light source for methane gas detection[20].

Methane gas molecules have absorption lines in both near-infrared and mid-infrared bands. The absorption coefficient of the absorption lines of carbon dioxide and water molecules near 1.65 μm is much smaller than that of methane molecules[22]. Therefore, the 1.65 μm light source is less affected by carbon dioxide and water molecules in the atmosphere, and its transmission loss is small. It is suitable for the long-distance detection of methane gas molecules. Compared with 3.3 μm and 7.66 μm lasers, 1.65 μm lasers have lower temperature requirements, which can reduce the complexity of detection equipment[23–26]. Close to the optical communication band, the corresponding optical devices and technologies of the 1.65 μm band are more mature.

A laser in the 1.6 μm band is designed as a potential light source for methane gas detection. It is required that the laser operates single mode lasing without mode hopping in the wavelength tuning range covering the methane absorption line at 1653.72 nm. The laser structure of a square microcavity as a WGM microcavity coupled with a Fabry–Pérot (FP) cavity meets the requirements and has the advantages of narrow linewidth, high side mode suppression ratio (SMSR), stable output wavelength, low power consumption, small volume, simple structure, and so on[27–29]. The coupled cavity laser eliminates the process of the second epitaxial growth method and is fabricated without high-precision lithography technology. It is edge emitting, which is conducive to the integration of light sources and other devices. Therefore, the square-FP coupled cavity laser is suitable as the light source of methane gas detection system based on TDLAS technology.

In this Letter, we report a square-FP coupled cavity semiconductor laser operating at about 1654 nm, corresponding to the methane absorption line. The laser output optical power can reach 7.4 mW with the SMSR about 40 dB, and the linewidth is 5 MHz at 1653.72 nm. The wavelength tunable properties

© 2022 Chinese Optics Letters

of the coupled cavity laser were analyzed. The lasing wavelength can be tuned by adjusting the FP cavity injection current covering a 2 nm tuning range, and it can also be tuned by adjusting the square microcavity injection current or temperature, respectively. A gas detection system based on TDLAS technology using the coupled cavity laser was demonstrated and used for methane gas detection.

2. Device Structure Simulation and Fabrication

We numerically simulate the field distributions of the magnetic component in hertz (Hz) for transverse electric (TE) polarized modes of a 2D square-FP coupled cavity with an FP cavity length of 300 μm and width of 2.5 μm as well as a square microcavity side length of 15 μm by the finite element method in the commercial software COMSOL Multiphysics 5.0. The coupled cavity with refractive index $n_1 = 3.2$ is surrounded by benzocyclobutene (BCB) with $n_2 = 1.54$, as shown in Fig. 1. The square microcavity and the FP cavity operate single mode and multi-mode lasing in the gain bandwidth, respectively, because of different free spectral ranges. When a vertex of the square microcavity and FP cavity are connected, resonance enhancement can be realized at the mode wavelength that meets the resonance conditions of the square microcavity and FP cavity at the same time. Coupled modes with higher Q factor obtained by hybridizing the WGM and FP mode realize high-power directional output via the FP cavity. TE mode distributions of the fundamental, first-order, and second-order modes in the square microcavity coupled with the mode in the FP microcavity are shown in Fig. 2, with mode wavelengths of 1642.8, 1641.47, and 1641.0 nm and Q factors of 1.91×10^4, 8.59×10^3, and 6.70×10^3, respectively. Compared with the first-order and second-order modes, the fundamental mode in the square microcavity coupled with the mode in the FP microcavity can achieve a higher Q factor, which indicates that the coupled cavity laser easily realizes single mode lasing.

An AlGaInAs/InP multiple-quantum-well laser wafer is used to fabricate the coupled cavity laser. The laser adopts the structure of numerical simulation above, as shown in Fig. 1. First, a 600 nm SiO_2 layer is deposited by plasma-enhanced chemical vapor deposition (PECVD) on the laser wafer. The patterns of the coupled cavity are transferred onto this SiO_2 layer using standard photolithography and inductively coupled plasma (ICP) etching techniques, and then the laser wafer is etched at about 4 μm by ICP etching with the patterned SiO_2 layer

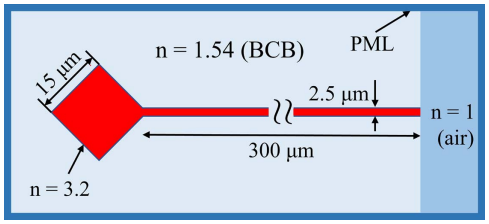

Fig. 1. Square-FP coupled cavity 2D structure schematic.

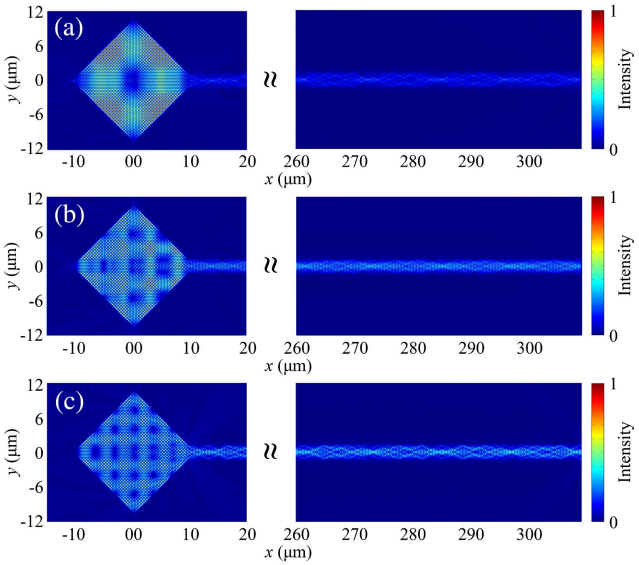

Fig. 2. TE mode distributions of the coupled cavity at different wavelengths. (a) 1642.8 nm; (b) 1641.47 nm; (c) 1641.0 nm.

as masks. The residual SiO_2 masks on the cavities were removed by using diluted HF solution. Next, a 250 nm SiN_x protecting layer is deposited by PECVD on the wafer, and a divinylsiloxane BCB (DVS-BCB) polymer overcladding layer is subsequently spun onto the SiN_x layer. The hard cured BCB layer is etched by reactive ion etching to expose the top of the microcavity structures. An electrically isolated channel is formed by ICP etching over the ohmic contact layer with the patterned SiO_2 mask layer obtained by the same method. A 200 nm SiO_2 insulating layer is deposited on the wafer, which can protect the isolated channel. Finally, SiO_2 and SiN_x on the top of the microcavity are removed by ICP etching to form an electrical injection window, and the patterned Ti-Pt-Au p-electrode is formed by photolithography and lift-off techniques. An Au-Ge-Ni metallization layer is evaporated on the backside as the n-electrode after the wafer mechanically laps down to a thickness of 120 μm. The laser wafer is cleaved to provide a reflection facet at the end of the FP cavity, with an FP cavity length of about 300 μm. A microscopic image of a laser chip is shown in Fig. 3(a). This laser chip contains two devices. This Letter is completed with only one device—laser A. The laser chip was sintered and wedge bonded on an AlN submount for subsequent testing. Figure 3(b) shows a microscope image of the laser after wedge bonding.

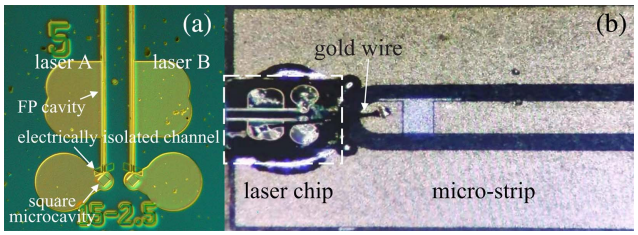

Fig. 3. Microscope image of the square-FP coupled cavity laser (a) after cleaving and (b) after wedge bonding.

3. Device Characteristics

The coupled cavity laser is tested on a semiconductor thermoelectric cooler (TEC), which is fixed at 16°C except for the variable temperature test. A multi-mode fiber is used to collect the output light at the output facet of the FP cavity away from the square microcavity except for the linewidth characterization. The injection currents of the two p-electrodes of the coupled cavity can be adjusted, respectively, when the laser operates. When the square microcavity injection current I_{SQ} is 20 mA, the output power of the laser at different FP cavity injection currents I_{FP} is shown in Fig. 4, and the threshold current is 16 mA. The multi-mode fiber coupling output power of the laser almost reaches a maximum of 7.4 mW at $I_{SQ} = 20$ mA and $I_{FP} = 84$ mA. The output power of the laser with the variation of I_{SQ} at fixed $I_{FP} = 83$ mA is shown in the inset of Fig. 4. The output optical power increases suddenly near $I_{SQ} = 0$ because the accumulation of photon generated carrier numbers causes saturation in the square microcavity. Affected by the increase of I_{SQ}, the equivalent reflectance of the square microcavity and the Q factor of the coupled modes increase, which causes the output power to increase until thermal saturation. As I_{SQ} continues to increase, the output power decreases slightly because of the thermal crosstalk between the square microcavity and FP cavities. The dominant mode wavelength is 1653.72 nm with the SMSR of 36.6 dB, as shown in the optical spectrum in Fig. 5, corresponding to the methane R3 absorption branch in the $2\nu_3$ second harmonic band.

The injection currents of the two p-electrodes of the coupled cavity, I_{SQ} and I_{FP}, are adjusted, respectively, to characterize the wavelength tunability of the laser. Optical spectra and SMSR of the laser with the variation of I_{FP} at fixed $I_{SQ} = 20$ mA are shown in Fig. 6(a). The wavelength tuning range is 2 nm from 1652.68 to 1654.70 nm by increasing I_{FP} from 66 to 98 mA with the step of 1 mA, covering the methane absorption line at 1653.72 nm, and the wavelength tuning rate of the current I_{FP} is 0.06 nm/mA. The laser operates single mode lasing without mode hopping

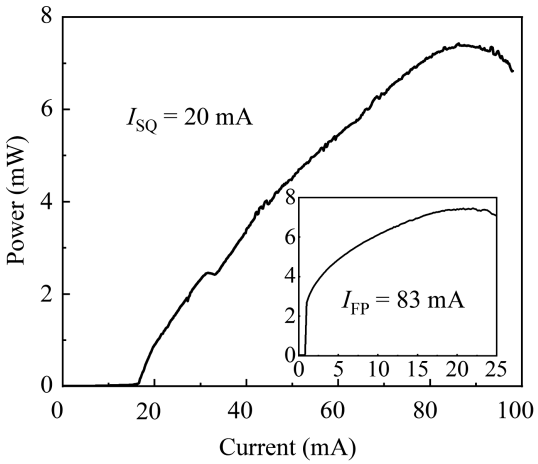

Fig. 4. Output optical power with the variation of I_{FP} at $I_{SQ} = 20$ mA. Inset: the output optical power with the variation of I_{SQ} at $I_{FP} = 83$ mA.

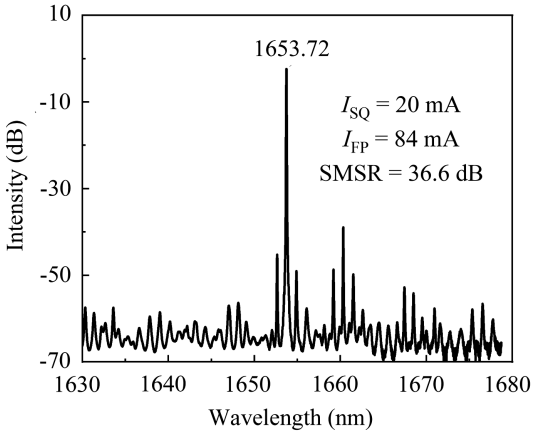

Fig. 5. Optical spectrum of the laser at injection current of $I_{SQ} = 20$ mA and $I_{FP} = 84$ mA.

with the SMSR almost above 40 dB. Optical spectra of the laser with the variation of I_{SQ} at fixed $I_{FP} = 83$ mA are shown in Fig. 6(b). The lasing wavelength is tuned from 1653.66 to 1653.74 nm by increasing I_{SQ} from 20 to 22 mA with the SMSR at about 42 dB, and the wavelength tuning rate of the current I_{SQ} is 0.04 nm/mA.

The lasing wavelength can also be tuned by adjusting the temperature except for adjusting the injection current, and it is red-shifted with increasing temperature. This is because the energy band structure and Fermi distribution in semiconductors are temperature dependent, and the active region gain peak and material refractive index change with temperature. For the

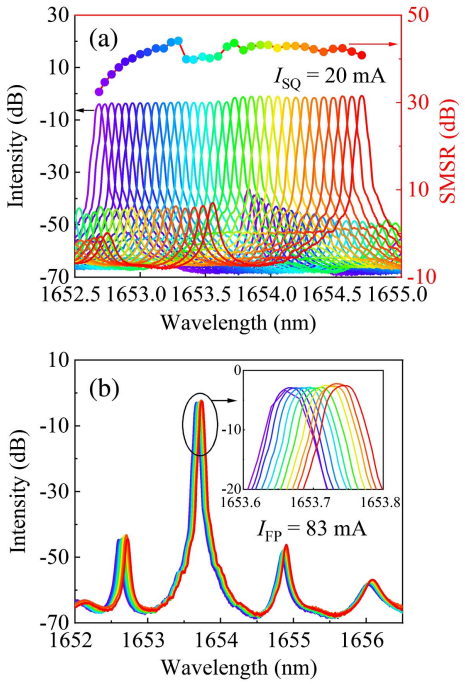

Fig. 6. (a) Optical spectra and SMSR with the variation of I_{FP} at $I_{SQ} = 20$ mA; (b) spectra with the variation of I_{SQ} at $I_{FP} = 83$ mA.

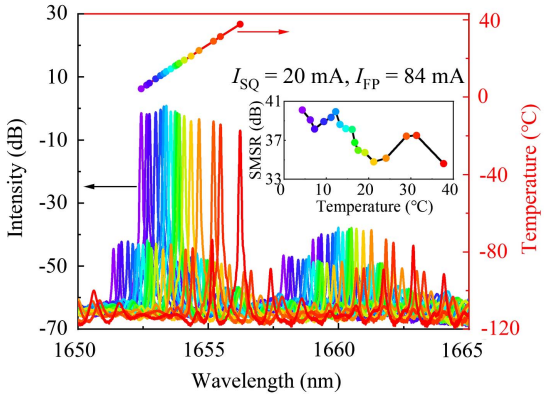

Fig. 7. Optical spectra and SMSR of the laser with the variation of temperature from 4.3°C to 37.7°C.

coupled cavity laser, the lasing wavelength shift with temperature depends on material refractive index variation, rather than the gain spectrum shift. Optical spectra and SMSR of the laser with temperature variation of the TEC at $I_{SQ} = 20$ mA and $I_{FP} = 84$ mA are shown in Fig. 7. The wavelength tuning range is 3.8 nm from 1652.43 to 1656.22 nm by increasing temperature of the TEC from 4.3°C to 37.7°C, and the wavelength tuning rate of the temperature is 0.11 nm/K. The laser operates single mode lasing without mode hopping, and the SMSR decreases from 40 dB to 35 dB.

The linewidth of the coupled cavity laser is characterized at $I_{SQ} = 20$ mA and $I_{FP} = 84$ mA, corresponding to the methane absorption line 1653.72 nm (R3-2ν_3) using the delay self-heterodyning method. The linewidth is a half of FWHM of 5 MHz, as shown in Fig. 8, which is much smaller than the FWHM of the methane absorption line.

4. Methane Gas Detection

A gas detection system based on TDLAS technology using the coupled cavity laser proposed in this Letter was built for

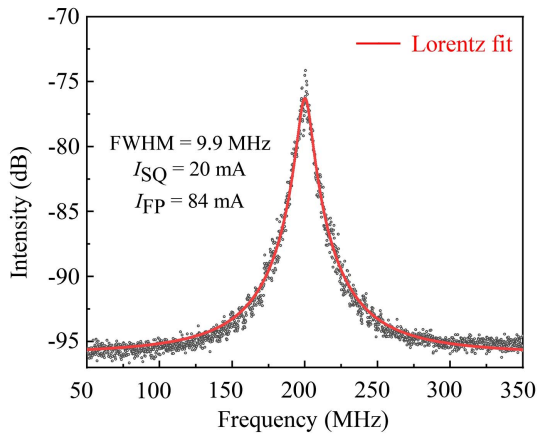

Fig. 8. Linewidth of the laser at injection current of I_{SQ} = 20 mA and I_{FP} = 84 mA.

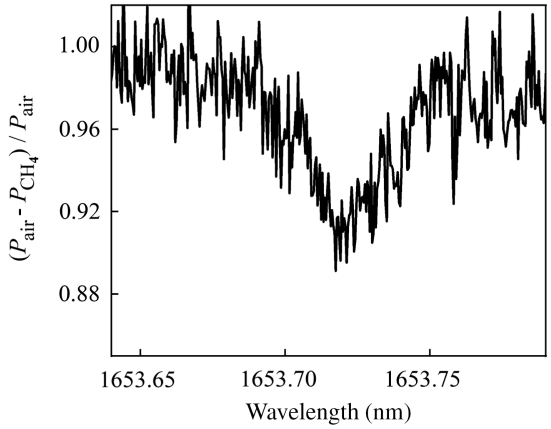

Fig. 9. $(P_{air}-P_{CH4})/P_{air}$ with the variation of the lasing wavelength.

methane gas detection. A white cell is used as the gas absorption cell. The sample gas is methane with a concentration of 1001 ppm (parts per million), and its equilibrium gas is nitrogen. The gas cell is filled with air before the sample gas is inlet. The lasing wavelength is tuned from 1653.65 to 1653.8 nm by adjusting I_{FP}, I_{SQ}, or temperature of the TEC, respectively. The output light of the coupled cavity laser is inlet from one end of the gas cell through a single mode fiber and collected by a detector at the other end of the gas cell. When the lasing wavelength is the same as the position of the methane absorption line, the gas molecules will absorb photons and move to a higher energy level, and the laser energy will decay at the same time. Methane gas detection can be realized by comparing the output optical power after absorption with the initial output optical power. Figure 9 shows the ratio of the difference of the output optical power received by the detector before and after sample gas inletting to the output optical power before sample gas inletting, that is, $(P_{air} - P_{CH4})/P_{air}$ as the lasing wavelength varies. The methane gas inlet caused a significant decrease in the output optical power at the methane absorption line of 1653.72 nm (R3-2ν_3).

5. Conclusion

In this Letter, methane gas detection is successfully demonstrated utilizing a square-FP coupled cavity laser. The coupled cavity laser operates at about 1654 nm, corresponding to the methane absorption line. The laser can operate single mode lasing with the SMSR about 40 dB and the linewidth of 5 MHz, and optical power can reach 7.4 mW. The lasing wavelength can be tuned by adjusting I_{FP}, I_{SQ}, or temperature of the TEC, respectively, and the laser operates single mode lasing without mode hopping. The fabricated square-FP coupled cavity laser is a high-performance laser source for methane gas detection.

Acknowledgement

This work was supported by the National Key R&D Program of China (No. 2017YFB0405301).

References

1. D. F. Swineharf, "The Beer–Lambert law," J. Chem. Educ. **39**, 333 (1962).
2. P. Werle, "A review of recent advances in semiconductor laser based gas monitors," Spectrochim. Acta A Mol. Biomol. Spectrosc. **54**, 197 (1998).
3. P. Werle, F. Slemr, K. Maurer, R. Kormann, R. Mucke, and B. Janker, "Near- and mid-infrared laser-optical sensors for gas analysis," Opt. Laser. Eng. **37**, 101 (2002).
4. N. S. Lawrence, "Analytical detection methodologies for methane and related hydrocarbons," Talanta **69**, 385 (2006).
5. M. Lackner, "Tunable diode laser absorption spectroscopy (TDLAS) in the process: a review," Rev. Chem. Eng. **23**, 65 (2007).
6. J. Shemshad, S. M. Aminossadati, and M. S. Kizil, "A review of developments in near infrared methane detection based on tunable diode laser," Sensor. Actuat. B Chem. **171**, 77 (2012).
7. J. Kamieniak, E. P. Randviir, and C. E. Banks, "The latest developments in the analytical sensing of methane," TrAC Trend. Anal. Chem. **73**, 146 (2015).
8. S. V. Kireev and S. L. Shnyrev, "On-line monitoring of odorant in natural gas mixtures of different composition by the infrared absorption spectroscopy method," Laser Phys. Lett. **15**, 035705 (2018).
9. F. Wang, S. Jia, Y. Wang, and Z. Tang, "Recent developments in modulation spectroscopy for methane detection based on tunable diode laser," Appl. Sci. **9**, 2816 (2019).
10. J. Mi, H. Yu, L. Yuan, S. Li, M. Li, S. Liang, Q. Kan, and J. Pan, "Distributed Bragg reflector laser (1.8 μm) with 10 nm wavelength tuning range," Chin. Opt. Lett. **13**, 041401 (2015).
11. H. Yu, P. Wang, J. Mi, X. Zhou, J. Pan, H. Wang, L. Xie, and W. Wang, "1.8-μm DBR lasers with over 11-nm continuous wavelength tuning range for multi-species gas detection," in *Asia Communications and Photonics Conference (ACP)* (2017), p. 1.
12. H. Yu, J. Pan, X. Zhou, H. Wang, L. Xie, and W. Wang, "A widely tunable three-section DBR lasers for multi-species gas detection," Appl. Sci. **11**, 2618 (2021).
13. H. Yu, M. Wang, D. Zhou, X. Zhou, P. Wang, S. Liang, Y. Zhang, J. Pan, and W. Wang, "A 1.6-μm widely tunable distributed Bragg reflector laser diode based on InGaAs/InGaAsP quantum-wells material," Opt. Commun. **497**, 127201 (2021).
14. Y. Fu, H. Liu, Y. Sui, B. Li, W. Ye, C. Zheng, and Y. Wang, "A near-infrared methane detection system using a 1.654 μm wavelength-modulated diode laser," Optoelectron. Lett. **12**, 140 (2016).
15. J. Wang, B. Li, G. Lin, Q. Ma, S. Wang, and M. Piao, "Near-infrared methane sensor based on a distributed feedback laser," Spectrosc. Lett. **52**, 113 (2019).
16. L. Shao, B. Fang, F. Zheng, X. Qiu, Q. He, J. Wei, C. Li, and W. Zhao, "Simultaneous detection of atmospheric CO and CH_4 based on TDLAS using a single 2.3 μm DFB laser," Spectrochim. Acta A Mol. Biomol. Spectrosc. **222**, 117118 (2019).
17. B. Wang, H. Lu, A. Li, Y. Chen, T. Dai, S. Huang, and H. Lian, "Research of TDLAS methane detection system using VCSEL laser as the light source," Infrared Laser Eng. **49**, 0405002 (2020).
18. M. Chen, Y. Shi, R. Xiao, Z. Sun, S. Chen, Y. Xu, B. Yang, and X. Chen, "Tunable DFB laser array for multi-gas detection," in *19th International Conference on Optical Communications and Networks (ICOCN)* (2021), p. 1.
19. B. Li, L. Xue, N. Ji, and D. Wei, "Research on spectroscopy modulation of a distributed feedback laser diode based on the TDLAS technique," Int. J. Opt. **2021**, 8829790 (2021).
20. F. Meng, H. Yu, X. Zhou, Y. Li, M. Wang, W. Yang, W. Chen, Y. Zhang, and J. Pan, "Quantum wells micro-ring resonator laser emitting at 1746 nm for gas sensing," Chin. Opt. Lett. **19**, 041406 (2021).
21. H. Lian, B. Wang, Y. Yu, L. Cheng, T. Dai, and S. Huang, "Carbon monoxide gas detection system based on VCSEL using TDLAS technology," Proc. SPIE **11887**, 118871O (2021).
22. I. E. Gordon, L. S. Rothman, C. Hill, R. V. Kochanov, Y. Tan, P. F. Bernath, M. Birk, V. Boudon, A. Campargue, K. V. Chance, B. J. Drouin, J. M. Flaud, R. R. Gamache, J. T. Hodges, D. Jacquemart, V. I. Perevalov, A. Perrin, K. P. Shine, M. A. H. Smith, J. Tennyson, G. C. Toon, H. Tran, V. G. Tyuterev, A. Barbe, A. G. Csaszar, V. M. Devi, T. Furtenbacher, J. J. Harrison, J. M. Hartmann, A. Jolly, T. J. Johnson, T. Karman, I. Kleiner, A. A. Kyuberis, J. Loos, O. M. Lyulin, S. T. Massie, S. N. Mikhailenko, N. Moazzen-Ahmadi, H. S. P. Muller, O. V. Naumenko, A. V. Nikitin, O. L. Polyansky, M. Rey, M. Rotger, S. W. Sharpe, K. Sung, E. Starikova, S. A. Tashkun, J. Vander Auwera, G. Wagner, J. Wilzewski, P. Wcislo, S. Yu, and E. J. Zak, "The HITRAN2016 molecular spectroscopic database," J. Quant. Spectrosc. Radiat. Transfer **203**, 3 (2017).
23. T. Hosoda, G. Kipshidze, L. Shterengas, and G. Belenky, "Diode lasers emitting near 3.44 μm in continuous-wave regime at 300 K," Electron. Lett. **46**, 1455 (2010).
24. L. Naehle, S. Belahsene, M. von Edlinger, M. Fischer, G. Boissier, P. Grech, G. Narcy, A. Vicet, Y. Rouillard, J. Koeth, and L. Worschech, "Continuous-wave operation of type-I quantum well DFB laser diodes emitting in 3.4 μm wavelength range around room," Electron. Lett. **47**, 46 (2011).
25. G. K. Veerabathrana, S. Sprengel, A. Andrejew, and M.-C. Amann, "Room-temperature vertical-cavity surface-emitting lasers at 4 μm with GaSb-based type-II quantum wells," Appl. Phys. Lett. **110**, 071104 (2017).
26. H. Nie, F. Wang, J. Liu, K. Yang, B. Zhang, and J. He, "Rare-earth ions-doped mid-infrared (2.7–3 μm) bulk lasers: a review," Chin. Opt. Lett. **19**, 091407 (2021).
27. X. Ma, Y. Huang, Y. Yang, J. Xiao, H. Weng, and Z. Xiao, "Mode coupling in hybrid square-rectangular lasers for single mode operation," Appl. Phys. Lett. **109**, 071102 (2016).
28. X. Ma, Y. Huang, Y. Yang, H. Weng, J. Xiao, M. Tang, and Y. Du, "Mode and lasing characteristics for hybrid square-rectangular lasers," IEEE J. Sel. Top. Quantum Electron. **23**, 1500409 (2017).
29. Y. Hao, F. Wang, M. Tang, H. Weng, Y. Yang, J. Xiao, and Y. Huang, "Widely tunable single-mode lasers based on a hybrid square/rhombus-rectangular microcavity," Photonics Res. **7**, 543 (2019).